Title: Shared and distinct brain regions targeted for immediate early gene expression by ketamine and psilocybin

Authors: Pasha A. Davoudian[1,2], Ling-Xiao Shao[3], Alex C. Kwan[3,4]*

Affiliations:
[1]Medical Scientist Training Program,
[2]Interdepartmental Neuroscience Program,
[3]Department of Psychiatry,
[4]Department of Neuroscience,
Yale University School of Medicine, New Haven, Connecticut, 06511, USA

Address correspondence to Alex Kwan, Ph.D., Department of Psychiatry, Yale University School of Medicine, 300 George St, Suite 901, New Haven, CT 06511, United States; E-mail: alex.kwan@yale.edu

Number of words in Abstract: 248
Number of words in Main Text: 3531

Short title: Brainwide c-Fos expression for psilocybin and ketamine

Keywords: Psychedelics, antidepressant, immediate early gene, c-Fos, activity-dependent transcription, neural plasticity

ABSTRACT

Background: Psilocybin is a psychedelic with therapeutic potential. While there is growing evidence that psilocybin exerts its beneficial effects through enhancing neural plasticity, the exact brain regions involved are not completely understood. Determining the impact of psilocybin on plasticity-related gene expression throughout the brain can broaden our understanding of the neural circuits involved in psychedelic-evoked neural plasticity.

Methods: Whole-brain serial two-photon microscopy and light sheet microscopy were employed to map the expression of the immediate early gene, c-Fos, in male and female mice. The drug-induced c-Fos expression following psilocybin administration was compared to that of subanesthetic ketamine and saline control. To gain insights into the contributions of receptors and cell types, the c-Fos expression maps were related to brain-wide *in situ* hybridization data.

Results: Psilocybin and ketamine produced acutely comparable elevations in c-Fos expression in numerous brain regions, including anterior cingulate cortex, locus coeruleus, primary visual cortex, central and basolateral amygdala, and claustrum. Select regions exhibited drug-preferential differences, such as dorsal raphe, lateral habenula, and insular cortex for psilocybin and retrosplenial cortex for ketamine. Correlation of psilocybin's effects with gene expression highlighted potential roles of 5-HT_{2A} and GluN2B subunit of NMDA receptors.

Conclusions: The systematic mapping approach produced an unbiased list of brain regions impacted by psilocybin and ketamine. The data are a valuable resource that highlights previously underappreciated regions for future investigations. By identifying regions with similar and disparate effects, the results provide insights into how psilocybin and ketamine may produce their rapid-acting and long-lasting therapeutic effects.

INTRODUCTION

Psychedelic compounds produce profound changes in states of perception, cognition, and consciousness (1,2). These compounds have been studied for their potential therapeutic effect for a variety of psychiatric conditions (3). In particular, psilocybin has reemerged recently with several promising early-phase clinical trials for the rapid and sustained treatment of depression (4–8). These results have led to an explosion of clinical trials to test the efficacy of psilocybin and other psychedelics as treatment for mental illnesses.

The therapeutic benefits of psychedelics are presumed to depend on neural plasticity (9–11). Most recent research to study psychedelics-induced neural plasticity has focused on the neocortex and hippocampus (12–19). However, as the compound is delivered systemically, many other regions in the brain can also potentially be responsive to psychedelic administration. Indeed, early work in rodents has shown strong responses to psychedelics in several subcortical nuclei. For example, the dorsal raphe, a key source of serotonin for the forebrain, exhibited a cessation of spiking activity following lysergic acid diethylamide (LSD) and other psychedelic compounds (20,21). Other studies demonstrated increased neural activity of the locus ceruleus in response to peripheral stimuli following ergoline and phenethylamine administration (22,23). Therefore, there is incentive to explore the entire brain to illuminate the neural circuits mediating the actions of psychedelics.

Immediate early genes such as c-Fos provide a window into the plasticity mechanisms evoked by psychedelics. Transcription is activated in neurons rapidly within minutes of stimulation, which could be due to spiking activity, but could also arise from exposure to growth factors (24) and can be pharmacologically induced (25,26). Importantly, immediate early genes are thought to mediate key steps in protein synthesis, synaptic potentiation, and structural plasticity (27,28). Not surprisingly, given the role of immediate early genes in neural plasticity, psychedelics have been demonstrated to increase expression of c-Fos when measured specifically as transcripts in the frontal cortex, hippocampus, and midbrain (29), and protein in the anterior cingulate cortex, paraventricular nucleus, bed nucleus of the stria terminalis, and central amygdala (30–34). However, these studies focused on pre-determined brain regions for analysis. New technologies such as serial two-photon microscopy and light-sheet microscopy enabled whole-brain mapping of c-Fos expression (35–38). In this study, we leveraged these technologies to map the brain-wide c-Fos expression distribution following the administration of psilocybin, comparing to the fast-acting antidepressant ketamine and saline controls.

METHODS AND MATERIALS

Animals

Equal numbers of male and female animals were used for the study. Animals were randomly assigned to the saline, ketamine, or psilocybin condition. No animals were excluded from data analysis. Adult, 6 to 20-week-old *cfos*^{GFP} mice (39,40) (B6.Cg-Tg(Fos-tTA,Fos-EGFP*)1Mmay/J, #018306, The Jackson Laboratory) were used for the serial two-photon whole-brain mapping experiments. Adult, 8-week-old C57BL/6J (#000664, The Jackson Laboratory) were used for the light sheet whole-brain mapping experiments. All animals were housed and handled according to protocols approved by the Institutional Animal Care and Use Committee (IACUC) at Yale University.

Serial two-photon microscopy – sample preparation and imaging

The *cfos*^{GFP} mice were injected with either saline (10 mL/kg, i.p.), ketamine (10 mg/kg, i.p.), or psilocybin (1 mg/kg, i.p.). At 3.5 hours after the injection, the mice were deeply anesthetized with isoflurane and transcardially perfused with phosphate buffered saline (P4417, Sigma-Aldrich) followed by paraformaldehyde (PFA, 4% in PBS). The brains were fixed in 4% PFA for 12 hours at 4°C. Brains were transferred to PBS with 0.1% sodium azide until they were sectioned and imaged. Whole-brain serial two-photon tomography imaging was performed using the previously described TissueCyte 1000 system (41). Briefly, brain samples were imaged using a laser with an excitation wavelength of 920 nm, and emitted fluorescence was captured across three channels (channel 1: 560–680, channel 2: 500–560, and channel 3: 400–500 nm). GFP fluorescence was detected in channel 2. Autofluorescence were identified in channel 1 and 3. Approximately 140 serial block-face images were acquired at 100-μm spacing for each brain at 1.4 μm/pixel XY sampling. The imaging steps were done blinded to the treatment conditions at TissueVision, Inc (Newton, MA).

Serial two-photon microscopy – analysis
Tiled brain images were processed through the QUINT workflow (42) for registration and quantification of c-Fos positive cells. First, images were registered to the Allen Brain Atlas (Allen Reference Atlas – Mouse Brain [Adult Mouse]. Available from atlas.brain-map.org) using the autofluorescence signals and QuickNII tool (43) was used to guide a rigid, affine registration and map brain slices into three-dimensional space based on key anatomical landmarks. Next, the VisuAlign tool (RRID:SCR_017978) was used to further improve the registration using nonlinear refinements. The c-Fos positive cells in each image were segmented with two levels of classification. An initial pixel-level classification and then an object-level classification performed via supervised machine-learning with *ilastik* (44). Lastly, the registered tiled brain images were overlaid with the segmented c-Fos positive cells using the Nutil tool (45) to determine count of c-Fos positive cells in each region.

Light-sheet microscopy – sample preparation and imaging
C57BL/6J mice were injected with either saline (10 mL/kg, i.p.), ketamine (10 mg/kg, i.p.), or psilocybin (1 mg/kg, i.p.). At 2 hours after the injection, the mouse was deeply anesthetized with isoflurane and transcardially perfused with phosphate buffered saline (P4417, Sigma-Aldrich) followed by paraformaldehyde (PFA, 4% in PBS). The brains were fixed in 4% PFA for 24 hours at 4°C. Brains were then transferred to PBS with 0.1% sodium azide until brain clearing and labeling. Whole mouse brains were processed following the SHIELD protocol (46). Samples were cleared for 1 day at 42°C with SmartBatch+ (LifeCanvas Technologies), a device employing stochastic electrotransport (47). Cleared samples were then actively immunolabeled using eFLASH technology integrating stochastic electrotransport (47) and SWITCH (48). Each brain sample was stained with primary antibodies, 3.5 mg of rabbit anti-c-Fos monoclonal antibody (Abcam, #ab214672), and 10 mg of mouse anti-NeuN monoclonal antibody (Encor Biotechnology, #MCA-1B7) followed by fluorescently conjugated secondaries in 1:2 primary:secondary molar ratios (Jackson ImmunoResearch). After active labeling, samples were incubated in EasyIndex (LifeCanvas Technologies) for refractive index matching (n = 1.52) and imaged at a magnification of 3.6X with a SmartSPIM light sheet microscope (LifeCanvas Technologies) at 1.8 µm/pixel XY sampling with 4 µm Z sampling over the entire brain. The imaging steps were done blinded to the treatment conditions at LifeCanvas Technologies (Cambridge, MA).

Light-sheet microscopy – analysis
Images were tile corrected, de-striped, and registered to the Allen Brain Atlas using an automated process. Specifically, a NeuN channel for each brain was registered to 8-20 atlas-aligned reference samples, using successive rigid, affine, and b-spline warping algorithms with SimpleElastix (49). An average alignment to the atlas was generated across all intermediate reference sample alignments to serve as the final atlas alignment value for the individual sample. Automated cell detection was performed using a custom convolutional neural network through the TensorFlow python package (50). The cell detection was performed by two networks in sequence. First, a fully-convolutional detection network (51) based on a U-Net architecture (52) as used to find possible locations of c-Fos positive cells. Second, a convolutional network using a ResNet architecture (53) was used to classify each location as positive or negative hit. Using the atlas registration, each cell location was projected onto the Allen Brain Atlas to quantify the number of c-Fos positive cells for each atlas-defined region.

Bridging serial two-photon and light-sheet imaging data
The Allen Mouse Brain Common Coordinate Framework (Allen CCF) contains over one thousand brain region delineations that are arranged hierarchically (54). To constrain our results, we focus our analysis here on the 316 'summary structures' as proposed by the Allen CCF authors (54). Owing to the lower axial sampling of the serial two-photon experiments, we included only brain regions where at least ten cells were detected in each brain analyzed across all drug treatment conditions. This resulted in the removal of 27 regions from the original set for a final dataset of 289 brain regions. To account for the variability of c-Fos expression across individuals (55), we scaled the c-Fos density of each region for each subject in the dataset by a factor consisting of the average c-Fos cell count for that region across all animals divided by the total cell count for that animal.

***In situ* hybridization**
We accessed publicly available *in situ* hybridization data of all mouse genes across the entire brain (56) to assess the relative expression of each gene in in each brain region via custom code through the AllenSDK (57,58). We used the regional density of RNA expression to quantify the expression of every gene in each

brain region of interest. For each gene, we further calculated the Pearson correlation coefficient between its regional expression levels with regional drug-induced differences in c-Fos expression.

Data and code availability

The data that support the findings and the code used to analyze the data in this study will be made publicly available at https://github.com/Kwan-Lab. Raw image files are terabytes in size and will be available upon request.

RESULTS

Whole-brain imaging of c-Fos expression

Mice received either saline (10 mL/kg, i.p.; n = 4 males, 4 females), ketamine (10 mg/kg, i.p. ; n = 4 males, 4 females), or psilocybin (1 mg/kg, i.p. ; n = 4 males, 4 females). A subanesthetic dose of 10 mg/kg was chosen for ketamine because prior work demonstrated that this dose is sufficient to evoke spinogenesis in the medial frontal cortex and reduce depressive-like behavior (59,60). A dose of 1 mg/kg was chosen for psilocybin because recent studies showed that this dose induce head-twitch response, increase dendritic spine formation, and enhance excitatory neurotransmission in the medial frontal cortex and hippocampus (12,13). To measure the acute impact of these drugs on the whole-brain expression of c-Fos, we used two complementary imaging methods. First, we used the *cfos*^{GFP} transgenic mouse (39,40) (**Figure 1A**) with the brain harvested 3.5 hr after drug administration, because we estimated 0.5 hr for peak effect of psilocybin and the fluorescent signal, arising from a two-hour half-life GFP associated with the c-Fos promoter, peaked at 3 hr in this particular transgenic mouse line (35). The fixed brain was imaged with serial two-photon microscopy (**Figure 1B**). This approach allowed us to examine GFP expression in the whole brain with micron-scale resolution (**Figure 1C**). The strength of this method is that the tissue does not need to be cleared, and therefore minimizes distortion. Second, we used the C57BL/6J mouse (Figure 1D), with the brain collected 2 hr after drug administration, because we estimated 0.5 hr for peak effect of ketamine and endogenous c-Fos protein expression accumulates over 1.5 hr (55,61). Whole-brain clearing and immunohistochemistry were used to label the endogenous c-Fos protein (**Figure 1D**). The cleared brain was imaged using light-sheet microscopy (**Figure 1E**). This latter approach allowed for visualization of c-Fos protein expression at a similar micron-scale resolution (**Figure 1F**). The strength of this method is the whole brain is sampled. Moreover, antibodies tag endogenously produced c-Fos proteins, which avoids potential confounds in using mutant animals where the transgene expression may not reflect endogenous c-Fos levels (62,63). Knowing the strengths and caveats of each method, the use of both techniques allowed us to generate complementary datasets to examine c-Fos expression differences.

Mapping drug-induced differences in c-Fos expression

We first examined the total number of c-Fos positive cells in each drug treatment condition and saline vehicle. Neither ketamine nor psilocybin induced significant differences in total c-Fos cell counts relative to saline (ketamine: $P = 0.95$; psilocybin: $P = 0.97$; two-sided *t*-test; **Figure 1G**). There was a significant difference in the total c-Fos positive cell count between the two imaging methods ($P = 3 \times 10^{-8}$, two-sided *t*-test, **Figure 1G**), as expected because serial two-photon microscopy sampled at only select axial positions, versus light-sheet microscopy which captured fluorescence signals from the entire cleared brain. We split the data by sex and did not detect difference between males and females in any condition ($P = 0.79$, two-sided *t*-test, **Figure 1H**).

Next, we analyzed the density of c-Fos positive cells divided by brain regions. We followed the guidance of Allen Mouse Brain Common Coordinate Framework, which identified 316 “summary structures” as the basis set for rodent brain parcellation (54). A number of brain regions, particularly tiny subcortical areas and sub-divisions of the cerebellum, have too few c-Fos positive cells; these regions were excluded (see Methods and Materials), leaving 289 regions for further analysis. **Figure 1I** shows the mean density of c-Fos positive cells in each region for the saline condition, separately plotted for the serial two-photon and light-sheet imaging data. We note the close correspondence of regional density for the two approaches, with the serial two-photon data being an approximately scaled version of the light-sheet data. To increase the number of samples per treatment condition, we will use normalized measures such as percent difference for subsequent analyses, allowing us to combine the results from the serial two-photon data and the light-sheet data.

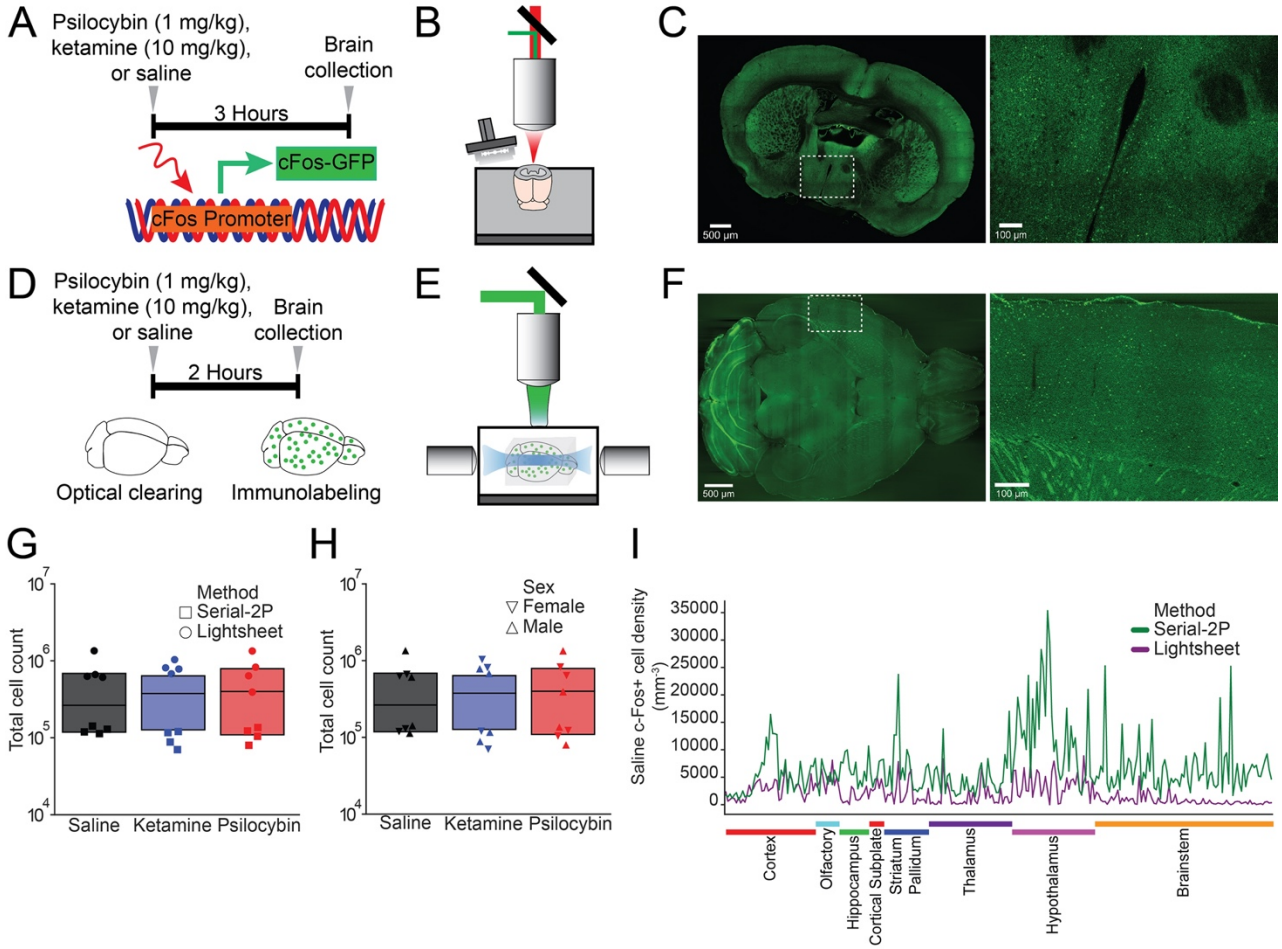

Figure 1. Whole-brain mapping of drug-induced c-Fos expression. (A) Transgenic c-Fos-GFP mice were injected with either saline, ketamine (10 mg/kg), or psilocybin (1 mg/kg) at 3 hours before sacrifice and collection of brains (*n* = 4 per condition). **(B)** Schematic of the serial two-photon microscope setup. **(C)** Left: tiled image of a coronal block-face of a brain from c-Fos-GFP mouse. Right: zoomed in view demonstrating expression of c-Fos puncta in neurons. **(D)** C57/BL6 mice were injected with either saline, ketamine (10 mg/kg), or psilocybin (1 mg/kg) at 2 hours before sacrifice and collection of brains (*n* = 4 per condition). Brains were cleared and then immunolabeled with antibody against c-Fos protein. **(E)** Schematic of the light-sheet microscope setup. **(F)** Left: image of a horizontal plane of a cleared mouse brain labeled with c-Fos antibody. Right: zoomed in view demonstrating expression of c-Fos puncta in neurons of the cortex. **(G)** Total number of c-Fos positive cells detected across different drug conditions and with the two imaging methods. Symbol, individual animal. Box plot shows the median, 25th and 75th percentiles. **(H)** Total number of c-Fos positive cells detected across different drug conditions and across sexes. Symbol, individual animal. Box plot shows the median, 25th and 75th percentiles. **(I)** The mean density of c-Fos positive cells (cells/mm^3) detected across brain regions in the saline condition using serial two-photon and light-sheet microscopy.

Psilocybin and ketamine induce convergent and distinct differences in c-Fos expression across brain regions

To focus on the effect of drug action, we calculated the percent difference in mean c-Fos positive cell density for either psilocybin or ketamine relative to saline (**Figure 2**). The brain regions were sorted based on their membership in higher-order groupings. This plot shows the heterogenous effects of psilocybin and ketamine on c-Fos expression on a region-by-region basis. Broadly, regions in the cortex, thalamus, and brainstem systems had substantial differences, whereas regions in the olfactory and striatum / pallidum systems have relatively modest differences. The mean c-Fos cell count and mean drug-induced percent change values are provided as spreadsheets in the **Supplement**.

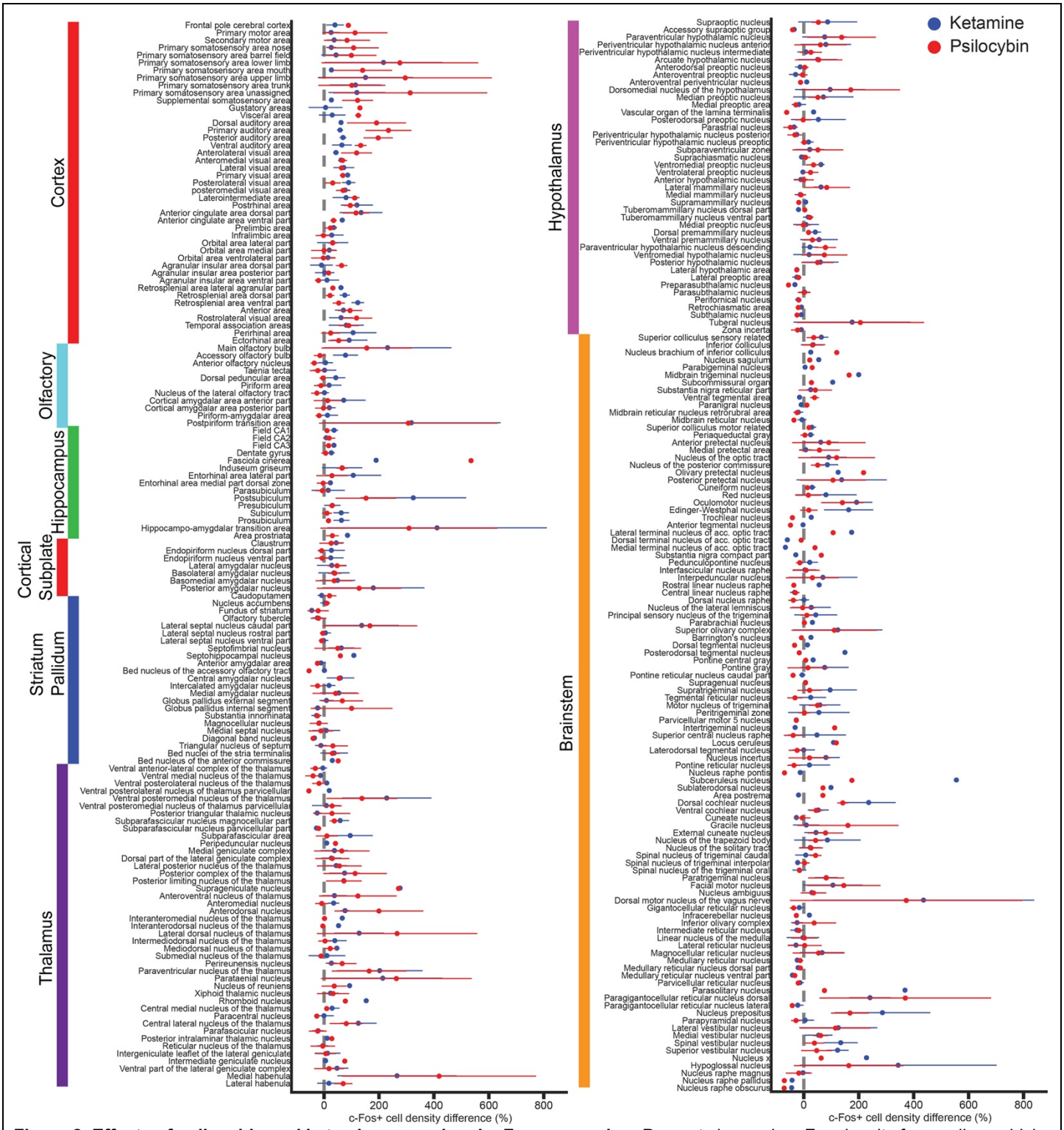

Figure 2. Effects of psilocybin and ketamine on regional c-Fos expression. Percent change in c-Fos density from saline vehicle baseline for psilocybin (red) and ketamine (blue). Circle, mean. Line, bootstrapped 95% confidence intervals assuming normal distribution.

To contrast effects of psilocybin and ketamine more clearly, we made a scatterplot of the average drug-induced c-Fos change by each drug (**Figure 3A**). For most brain regions examined, psilocybin and ketamine both increased c-Fos expression (upper right quadrant) or both decreased c-Fos expression (lower left quadrant, **Figure 3A**), although select locations showed preferential response to psilocybin or ketamine. We highlight several regions of interest in the neocortex, either because of prior studies or because of large drug-evoked effects. In the medial frontal cortex, psilocybin and ketamine induced the largest change in c-Fos expression for the dorsal regions (i.e., dorsal anterior cingulate cortex (ACAd; **Figure 3B**) and ventral anterior cingulate cortex (ACAv)), with smaller increases as a function of depth for the more ventral regions (i.e.,

prelimbic area (PL) and infralimbic area (ILA)). Psilocybin elicited greater elevation of c-Fos expression in several cortical regions such as ventral auditory area (AUDv), visceral area (VISC), frontal pole cerebral cortex (FRP), and the dorsal agranular insular area (AId; **Figure 3A, 3B**). Conversely, ketamine evoked larger differences in various retrosplenial cortical areas (RSPd, RSPv, RSPagl; **Figure 3A, 3B**). Intriguingly, psilocybin and ketamine were both effective at elevating the immediate early gene levels in the primary visual area (VISp).

Psilocybin and ketamine also have shared and divergent targets in subcortical regions of interest. The locus ceruleus (LC) was notable for large raises in c-Fos expression following both psilocybin and ketamine. Similarly, the claustrum (CLA) as well as several amygdalar (CEA, BLA, CLA) and midline thalamic nuclei (RE, MD) also exhibited increased c-Fos expression following ketamine or psilocybin. The lateral habenula (LH) and area postrema (AP) were more selectively targeted by psilocybin than ketamine. However, not all regions exhibited increases in c-Fos positive cells: both drugs were effective at suppressing c-Fos expression in the cholinergic diagonal band nucleus (NDB) and psilocybin was selective for decreasing c-Fos expression in the dorsal nucleus raphe (DR; **Figure 3B**) and nucleus raphe pontis (RPO). There are also regions with negligible change in c-Fos expression, such as the reticular nucleus of the thalamus (RT).

Several aspects of these results are consistent with prior work, which validate the whole-brain mapping approach. For instance, the medial frontal cortex, particularly the anterior cingulate cortex, is known to increase firing activity acutely following the systemic administration of NMDAR antagonists (17,64), including subanesthetic ketamine (65). Our identification of ketamine-specific increases of c-Fos signals in retrosplenial cortex is consistent with an earlier study using higher doses of ketamine (66) and a recent report of ketamine-evoked oscillatory activity in retrosplenial areas, especially in ventral regions (67). For psychedelics, a most telltale sign was the decrease in c-Fos expression in dorsal raphe, which echoes the classic finding of near-complete cessation of spiking activity following various psychedelics including psilocin (20,21,68). However, many characterized regions in this study were previously underappreciated as potential mediators of psilocybin's action. Preferential effect for psilocybin in insular area, which is implicated in interoception and emotional awareness (69), area postrema, which is involved in vomiting for humans, and lateral habenula, which is maladaptively affected by stress and depressive state (70–72), are a few examples of potential interest.

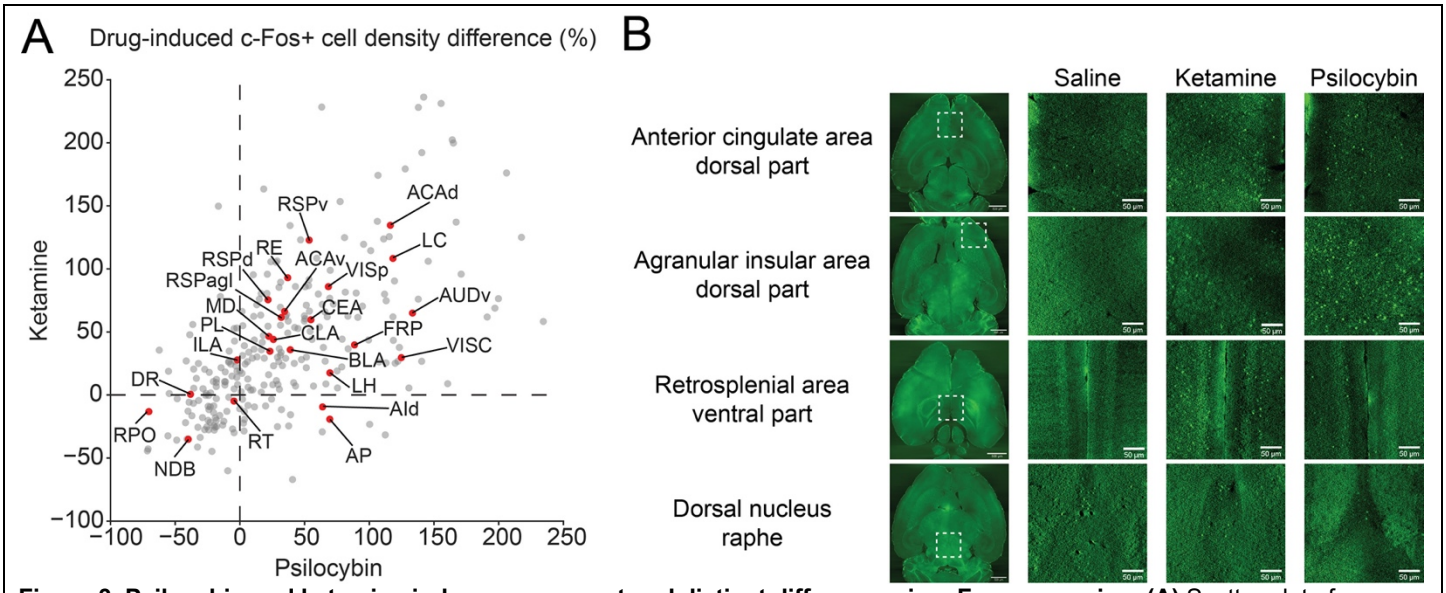

Figure 3. Psilocybin and ketamine induce convergent and distinct differences in c-Fos expression. (A) Scatter plot of mean percent change in c-Fos density from saline vehicle, for psilocybin (x-axis) versus ketamine (y-axis). ACAd: Anterior cingulate cortex, dorsal part. ACAv: Anterior cingulate cortex, ventral part. AId: Anterior insula, dorsal part. AP: Area Postrema. AUDv: Auditory area, ventral part. BLA:. Basolateral amygdala. CEA: Central amygdala. CLA: Claustrum. DR: Dorsal nucleus raphe. FRP: Frontal pole, cerebral cortex. ILA: Infralimbic area. LC: locus ceruleus.. LH: Lateral habenula. MD: mediodorsal thalamus. NDB: Nucleus of diagonal band. PL: Prelimbic area. RE: Nucleus of reuniens. RPO: Nulceus raphe pontis. RSPagl: Retrosplenial area, agranular part. RSPd: Retrosplenial area, dorsal part. RSPv: Retrosplenial area, ventral part. RT: Reticular nucleus of the thalamus. VISC: Visceral area. VISP: Primary visual cortex. **(B)** Example images from light-sheet microscopy for select cortical and subcortical brain areas. Due to background intensity, for visualization purposes, we performed gamma correction on the magnified images, using the same adjustment for each row of images.

Receptors and cell types that may contribute to drug-induced c-Fos expression

To gain insight into the mechanisms by which these complex pharmacological agents act, we analyzed our c-Fos expression data in reference to publicly available atlas of gene expression. We leveraged the Allen Brain Institute's *in situ* hybridization maps of the entire mouse brain (56), which has the mRNA transcript levels of all 19,413 genes in the mouse genome including various receptors and cell-type-specific markers. To estimate the relevance of each gene, we correlated its regional expression levels with the regional drug-evoked c-Fos expression (**Figure 4A**). When the analysis was applied to the entire brain, psilocybin-induced differences in c-Fos expression was correlated best with *Htr2a*, relative to any other serotonin receptor subtypes (**Figure 4B**). *Htr2a* encodes the 5-HT_{2A} receptor. Intriguingly, among the set of all serotonin receptors, dopamine receptors, and NMDA receptor subunits, the expression pattern of *Grin2b*, which encodes the GluN2B subunit of NMDA receptors, exhibited the highest correlation to the c-Fos expression maps for psilocybin (**Figure 4B**). By contrast, ketamine-induced differences in c-Fos did not correlate particularly well to any of our selected receptors on a brain-wide scale (**Figure 4C**). When restricting the analysis to only regions in the cortex, we found qualitatively similar results for psilocybin, with even higher correlations for *Grin2b*, *Gria2*, and *Htr2a* (**Figure 4D**). The *Grin2b* gene also had a much stronger correlation with ketamine-induced c-Fos expression across cortical regions (**Figure 4E**), corroborating recent studies showing the importance of GluN2B for ketamine's antidepressant action (65,73). Lastly, there are established genetic markers for various cell types in the cortex (74). We found several genes that correlated well with both psilocybin- and ketamine-induced differences in c-Fos expression: *Pvalb*, a marker for GABAergic fast-spiking interneurons, *Lamp5*, a marker for a subclass of GABAergic interneurons including neurogliaform cells and single bouquet cells, and *Fezf2*, a marker of extra-telencephalic projecting layer-5 pyramidal cells that include pyramidal tract neurons (**Figure 4F, G**). Cumulatively, this exploratory analysis highlights several receptors that may play a role in shaping the effects of psilocybin and ketamine on neural plasticity in specific cell types.

DISCUSSION

Our study revealed the similarities and differences in the expression of the immediate early gene c-Fos following administration of psilocybin and ketamine. The systematic, unbiased mapping approach provides a comprehensive coverage of all brain regions and should be a valuable resource for the community seeking to understand the effects of these compounds. For psilocybin, the data not only affirm the likely importance of well-studied brain regions such as the anterior cingulate cortex and dorsal raphe, but also pinpoint several underappreciated regions such as lateral habenula and insular cortex that may be crucial for drug action.

We chose c-Fos for this study, because it is a well-characterized immediate early gene and its nuclear staining is amenable to automated cell counting using machine learning tools. However, there are several limitations. First, the use of transgenic animals may yield signals that differ from the endogenous c-Fos expression. Such discrepancy was documented in a recent comparison following whisker learning in mice (63), and may due in part to numerous enhancers surrounding the c-Fos gene being important for response to stimuli (62). This caveat is alleviated in part in this study by also studying c-Fos expression in wild type mice using light-sheet microscopy. Second, c-Fos captures activity-dependent transcription in the nucleus, but drug-evoked neural plasticity is likely to also rely on local mechanisms, such as local protein synthesis in the dendritic compartments. Third, although c-Fos expression increases are widely thought to reflect elevated spiking activity, the relationship remains unclear. Our results broadly support this view, with ketamine's effect on anterior cingulate cortex and psilocybin's effect on dorsal raphe consistent to prior electrophysiological measurements. However, there are also discrepancies: for example, we observed psilocybin-induced c-Fos expression in medial frontal cortex and primary visual cortex, but studies indicate that the overall effects of psychedelics, at least for the phenethylamine DOI, on spiking activity should be suppressive in these regions (17,75). Finally, as an immediate early gene, the expression of c-Fos is expected to evolve over time. We have chosen a single time point to capture peak expression level, but future studies may include additional measurements to delineate a time course (76).

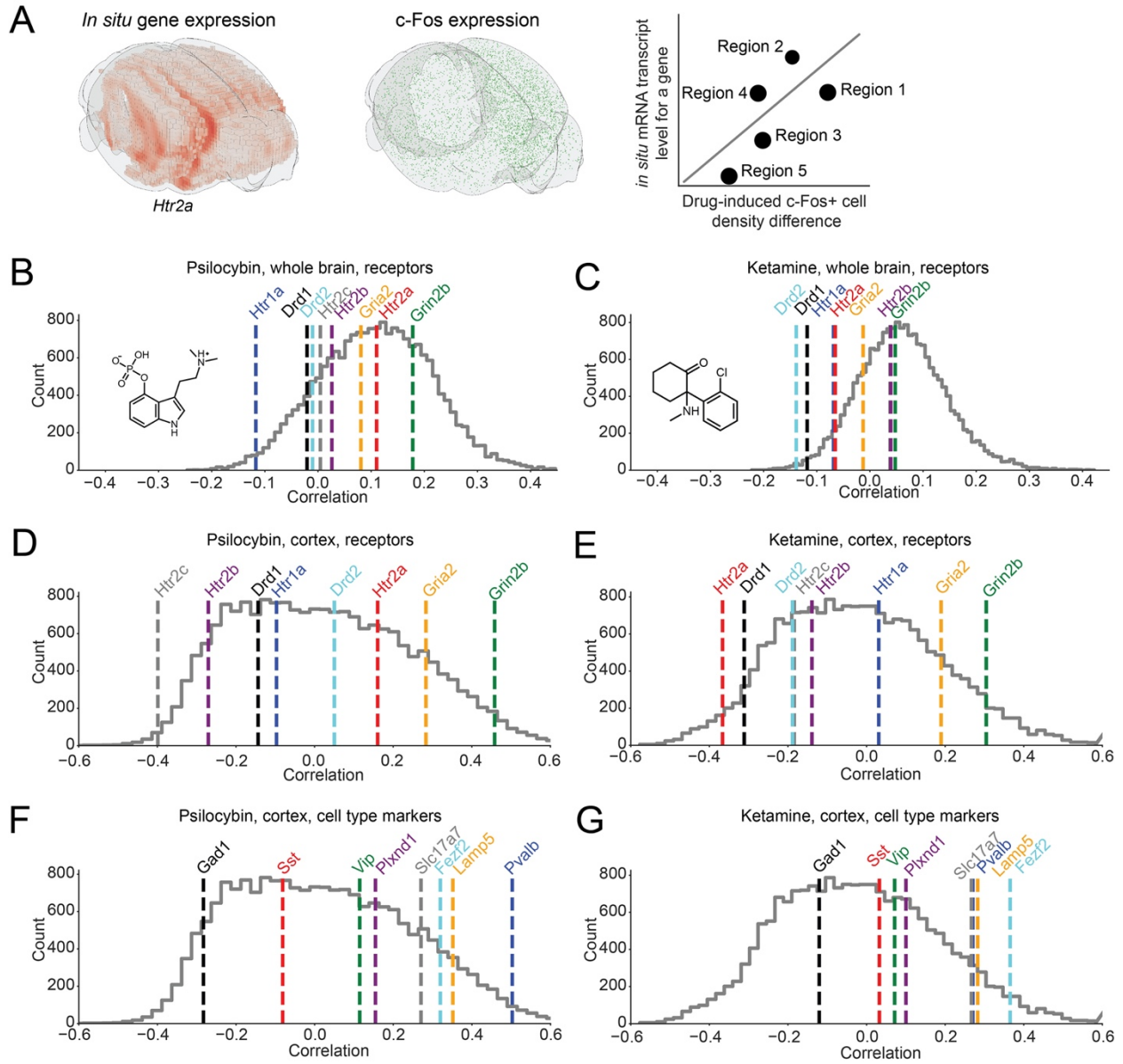

Figure 4. Potential receptors and cell types contributing to drug action. **(A)** Schematic illustrating the analysis procedure. The mRNA transcript levels of a particular gene (e.g., *Htr2a*) (left, interpolated from sagittal sections to yield 3D rendering) was compared with drug-induced percent change in density of c-Fos expression (middle), on a region-by-region basis to calculate a correlation coefficient (right). **(B)** Correlation coefficients computed for psilocybin condition using regions across the entire brain. Colored lines, correlation coefficients for specific receptor genes. Grey line, histogram of correlation coefficients for all 19,413 genes in the mouse genome. **(C)** Similar to (B) but for ketamine. **(D)** Similar to (B) but using regions within the cortex. **(E)** Similar to (D) but for ketamine. **(F)** Similar to (D), except colored lines indicate correlation coefficients for specific cell-type marker genes. **(G)** Similar to (F) but for ketamine.

Looking forward, the approach used here could be extended to study other drugs and new chemical entities. This may be other psychedelics, which include a large array of compounds (1,2) that vary in their binding affinity to various serotonin and non-serotonin receptors (77). The effects of psilocybin and ketamine may be compared to other antidepressant agents, such as brexanolone (78) and lumateperone (79), and new treatment options, such as other glutamate-targeting drugs (80,81) or nitrous oxide (82). Understanding the shared and disparate mechanisms underlying contrasting drugs will be crucial in developing a greater understanding of the pharmacology of rapid-acting antidepressants.

ACKNOWLEDGMENTS

We thank Neil Savalia, Adam Tyson, and Boris Heifets for discussions about the analysis. Psilocybin was generously provided by Usona Institute's Investigational Drug & Material Supply Program; the Usona Institute IDMSP is supported by Alexander Sherwood, Robert Kargbo, and Kristi Kaylo in Madison, WI. This work was supported by the Yale Center for Psychedelic Science, NIH/NIMH grant R01MH121848 (A.C.K.), and

NIH/NIGMS medical scientist training grant T32GM007205 (P.A.D.). This manuscript has been deposited as a preprint on the bioRxiv server.

DISCLOSURES

A.C.K. serves on the scientific advisory board for Empyrean Neuroscience. No-cost compounds were provided to A.C.K. for research by Usona Institute. The authors declare no other competing interests or disclosures.

REFERENCES

1. Nichols DE (2016): Psychedelics. *Pharmacol Rev* 68: 264–355.
2. Kelmendi B, Kaye AP, Pittenger C, Kwan AC (2022): Psychedelics. *Current Biology*.
3. Vollenweider FX, Preller KH (2020): Psychedelic drugs: neurobiology and potential for treatment of psychiatric disorders. *Nat Rev Neurosci* 1–14.
4. Carhart-Harris RL, Bolstridge M, Rucker J, Day CMJ, Erritzoe D, Kaelen M, *et al.* (2016): Psilocybin with psychological support for treatment-resistant depression: an open-label feasibility study. *Lancet Psychiatry* 3: 619–627.
5. Carhart-Harris R, Giribaldi B, Watts R, Baker-Jones M, Murphy-Beiner A, Murphy R, *et al.* (2021): Trial of Psilocybin versus Escitalopram for Depression. *New Engl J Med* 384: 1402–1411.
6. Griffiths RR, Johnson MW, Carducci MA, Umbricht A, Richards WA, Richards BD, *et al.* (2016): Psilocybin produces substantial and sustained decreases in depression and anxiety in patients with life-threatening cancer: A randomized double-blind trial. *J Psychopharmacol Oxf Engl* 30: 1181–1197.
7. Gukasyan N, Davis AK, Barrett FS, Cosimano MP, Sepeda ND, Johnson MW, Griffiths RR (2022): Efficacy and safety of psilocybin-assisted treatment for major depressive disorder: Prospective 12-month follow-up. *J Psychopharmacol* 36: 151–158.
8. Davis AK, Barrett FS, May DG, Cosimano MP, Sepeda ND, Johnson MW, *et al.* (2021): Effects of Psilocybin-Assisted Therapy on Major Depressive Disorder. *Jama Psychiat* 78: 481–489.
9. Aleksandrova LR, Phillips AG (2021): Neuroplasticity as a convergent mechanism of ketamine and classical psychedelics. *Trends Pharmacol Sci*. https://doi.org/10.1016/j.tips.2021.08.003
10. Savalia NK, Shao L-X, Kwan AC (2020): A Dendrite-Focused Framework for Understanding the Actions of Ketamine and Psychedelics. *Trends Neurosci*. https://doi.org/10.1016/j.tins.2020.11.008
11. Vargas MV, Meyer R, Avanes AA, Rus M, Olson DE (2021): Psychedelics and Other Psychoplastogens for Treating Mental Illness. *Frontiers Psychiatry* 12: 727117.
12. Shao L-X, Liao C, Gregg I, Davoudian PA, Savalia NK, Delagarza K, Kwan AC (2021): Psilocybin induces rapid and persistent growth of dendritic spines in frontal cortex in vivo. *Neuron* 109: 2535-2544.e4.
13. Hesselgrave N, Troppoli TA, Wulff AB, Cole AB, Thompson SM (2021): Harnessing psilocybin: antidepressant-like behavioral and synaptic actions of psilocybin are independent of 5-HT2R activation in mice. *Proc National Acad Sci* 118: e2022489118.
14. Revenga M de la F, Zhu B, Guevara CA, Naler LB, Saunders JM, Zhou Z, *et al.* (2021): Prolonged epigenomic and synaptic plasticity alterations following single exposure to a psychedelic in mice. *Cell Reports* 37: 109836–109836.
15. Cameron LP, Tombari RJ, Lu J, Pell AJ, Hurley ZQ, Ehinger Y, *et al.* (2021): A non-hallucinogenic psychedelic analogue with therapeutic potential. *Nature* 589: 474–479.
16. Lu J, Tjia M, Mullen B, Cao B, Lukasiewicz K, Shah-Morales S, *et al.* (2021): An analog of psychedelics restores functional neural circuits disrupted by unpredictable stress. *Mol Psychiatr* 26: 6237–6252.
17. Wood J, Kim Y, Moghaddam B (2012): Disruption of Prefrontal Cortex Large Scale Neuronal Activity by Different Classes of Psychotomimetic Drugs. *J Neurosci* 32: 3022–3031.
18. Gregorio DD, Popic J, Enns JP, Inserra A, Skalecka A, Markopoulos A, *et al.* (2021): Lysergic acid diethylamide (LSD) promotes social behavior through mTORC1 in the excitatory neurotransmission. *P Natl Acad Sci Usa* 118: e2020705118.
19. Dearnley B, Dervinis M, Shaw M, Okun M (n.d.): Stretching and squeezing of neuronal log firing rate distribution by psychedelic and intrinsic brain state transitions. https://doi.org/10.1101/2021.08.22.457198
20. Aghajanian GK, Foote WE, Sheard MH (1968): Lysergic Acid Diethylamide: Sensitive Neuronal Units in the Midbrain Raphe. *Science* 161: 706–708.
21. Aghajanian GK, Foote WE, Sheard MH (1970): Action of psychotogenic drugs on single midbrain raphe neurons. *J Pharmacol Exp Ther* 171: 178–87.

22. Aghajanian GK (1980): Mescaline and LSD facilitate the activation of locus coeruleus neurons by peripheral stimuli. *Brain Res* 186: 492–498.
23. Rasmussen K, Aghajanian GK (1986): Effect of hallucinogens on spontaneous and sensory-evoked locus coeruleus unit activity in the rat: reversal by selective 5-HT2antagonists. *Brain Res* 385: 395–400.
24. Greenberg ME, Ziff EB (1984): Stimulation of 3T3 cells induces transcription of the c-fos proto-oncogene. *Nature* 311: 433–438.
25. Hunt SP, Pini A, Evan G (1987): Induction of c-fos-like protein in spinal cord neurons following sensory stimulation. *Nature* 328: 632–634.
26. Morgan JI, Cohen DR, Hempstead JL, Curran T (1987): Mapping Patterns of c-fos Expression in the Central Nervous System After Seizure. *Science* 237: 192–197.
27. Morgan JI, Curran T (1989): Stimulus-transcription coupling in neurons: role of cellular immediate-early genes. *Trends Neurosci* 12: 459–462.
28. Sheng M, Greenberg ME (1990): The regulation and function of c-fos and other immediate early genes in the nervous system. *Neuron* 4: 477–485.
29. Nichols CD, Sanders-Bush E (2002): A Single Dose of Lysergic Acid Diethylamide Influences Gene Expression Patterns within the Mammalian Brain. *Neuropsychopharmacol* 26: 634–642.
30. Frankel PS, Cunningham KA (2002): The hallucinogen d-lysergic acid diethylamide (d-LSD) induces the immediate-early gene c-Fos in rat forebrain. *Brain Res* 958: 251–260.
31. González-Maeso J, Yuen T, Ebersole BJ, Wurmbach E, Lira A, Zhou M, *et al.* (2003): Transcriptome Fingerprints Distinguish Hallucinogenic and Nonhallucinogenic 5-Hydroxytryptamine 2A Receptor Agonist Effects in Mouse Somatosensory Cortex. *J Neurosci* 23: 8836–8843.
32. Erdtmann-Vourliotis M, Mayer P, Riechert U, Höllt V (1999): Acute injection of drugs with low addictive potential (Δ9-tetrahydrocannabinol, 3,4-methylenedioxymethamphetamine, lysergic acid diamide) causes a much higher c-fos expression in limbic brain areas than highly addicting drugs (cocaine and morphine). *Mol Brain Res* 71: 313–324.
33. Gresch PJ, Strickland LV, Sanders-Bush E (2002): Lysergic acid diethylamide-induced Fos expression in rat brain: role of serotonin-2A receptors. *Neuroscience* 114: 707–713.
34. Jefsen OH, Elfving B, Wegener G, Müller HK (2021): Transcriptional regulation in the rat prefrontal cortex and hippocampus after a single administration of psilocybin. *J Psychopharmacol* 35: 483–493.
35. Kim Y, Venkataraju KU, Pradhan K, Mende C, Taranda J, Turaga SC, *et al.* (2015): Mapping Social Behavior-Induced Brain Activation at Cellular Resolution in the Mouse. *Cell Reports* 10: 292–305.
36. Kim Y, Perova Z, Mirrione MM, Pradhan K, Henn FA, Shea S, *et al.* (2016): Whole-Brain Mapping of Neuronal Activity in the Learned Helplessness Model of Depression. *Front Neural Circuit* 10: 3.
37. Renier N, Adams EL, Kirst C, Wu Z, Azevedo R, Kohl J, *et al.* (2016): Mapping of Brain Activity by Automated Volume Analysis of Immediate Early Genes. *Cell* 165: 1789–1802.
38. Salinas CBG, Lu TT-H, Gabery S, Marstal K, Alanentalo T, Mercer AJ, *et al.* (2018): Integrated Brain Atlas for Unbiased Mapping of Nervous System Effects Following Liraglutide Treatment. *Sci Rep-uk* 8: 10310.
39. Reijmers LG, Perkins BL, Matsuo N, Mayford M (2007): Localization of a Stable Neural Correlate of Associative Memory. *Science* 317: 1230–1233.
40. Garner AR, Rowland DC, Hwang SY, Baumgaertel K, Roth BL, Kentros C, Mayford M (2012): Generation of a Synthetic Memory Trace. *Science* 335: 1513–1516.
41. Ragan T, Kadiri LR, Venkataraju KU, Bahlmann K, Sutin J, Taranda J, *et al.* (2012): Serial two-photon tomography for automated ex vivo mouse brain imaging. *Nat Methods* 9: 255–258.
42. Yates SC, Groeneboom NE, Coello C, Lichtenthaler SF, Kuhn P-H, Demuth H-U, *et al.* (2019): QUINT: Workflow for Quantification and Spatial Analysis of Features in Histological Images From Rodent Brain. *Front Neuroinform* 13: 75.
43. Puchades MA, Csucs G, Ledergerber D, Leergaard TB, Bjaalie JG (2019): Spatial registration of serial microscopic brain images to three-dimensional reference atlases with the QuickNII tool. *Plos One* 14: e0216796.
44. Berg S, Kutra D, Kroeger T, Straehle CN, Kausler BX, Haubold C, *et al.* (2019): ilastik: interactive machine learning for (bio)image analysis. *Nat Methods* 16: 1226–1232.
45. Groeneboom NE, Yates SC, Puchades MA, Bjaalie JG (2020): Nutil: A Pre- and Post-processing Toolbox for Histological Rodent Brain Section Images. *Front Neuroinform* 14: 37.
46. Park Y-G, Sohn CH, Chen R, McCue M, Yun DH, Drummond GT, *et al.* (2019): Protection of tissue physicochemical properties using polyfunctional crosslinkers. *Nat Biotechnol* 37: 73–83.

47. Kim S-Y, Cho JH, Murray E, Bakh N, Choi H, Ohn K, *et al.* (2015): Stochastic electrotransport selectively enhances the transport of highly electromobile molecules. *Proc National Acad Sci* 112: E6274–E6283.
48. Murray E, Cho JH, Goodwin D, Ku T, Swaney J, Kim S-Y, *et al.* (2015): Simple, Scalable Proteomic Imaging for High-Dimensional Profiling of Intact Systems. *Cell* 163: 1500–1514.
49. Marstal K, Berendsen F, Staring M, Klein S (2016): SimpleElastix: A User-Friendly, Multi-Lingual Library for Medical Image Registration. *2016 Ieee Conf Comput Vis Pattern Recognit Work Cvprw* 574–582.
50. Abadi M, Agarwal A, Barham P, Brevdo E, Chen Z, Citro C, *et al.* (2016): TensorFlow: Large-Scale Machine Learning on Heterogeneous Distributed Systems. *Arxiv*.
51. Shelhamer E, Long J, Darrell T (2016): Fully Convolutional Networks for Semantic Segmentation. *Arxiv*.
52. Ronneberger O, Fischer P, Brox T (2015): U-Net: Convolutional Networks for Biomedical Image Segmentation. *Arxiv*.
53. He K, Zhang X, Ren S, Sun J (2015): Deep Residual Learning for Image Recognition. *Arxiv*.
54. Wang Q, Ding S-L, Li Y, Royall J, Feng D, Lesnar P, *et al.* (2020): The Allen Mouse Brain Common Coordinate Framework: A 3D Reference Atlas. *Cell* 181: 936-953.e20.
55. Bullitt E (1990): Expression of C-fos-like protein as a marker for neuronal activity following noxious stimulation in the rat. *J Comp Neurol* 296: 517–530.
56. Lein ES, Hawrylycz MJ, Ao N, Ayres M, Bensinger A, Bernard A, *et al.* (2007): Genome-wide atlas of gene expression in the adult mouse brain. *Nature* 445: 168–176.
57. Fulcher BD, Murray JD, Zerbi V, Wang X-J (2019): Multimodal gradients across mouse cortex. *Proc National Acad Sci* 116: 201814144.
58. Fulcher BD, Fornito A (2016): A transcriptional signature of hub connectivity in the mouse connectome. *Proc National Acad Sci* 113: 1435–1440.
59. Wu M, Minkowicz S, Dumrongprechachan V, Hamilton P, Kozorovitskiy Y (2021): Ketamine Rapidly Enhances Glutamate-Evoked Dendritic Spinogenesis in Medial Prefrontal Cortex Through Dopaminergic Mechanisms. *Biol Psychiat* 89: 1096–1105.
60. Phoumthipphavong V, Barthas F, Hassett S, Kwan AC (2016): Longitudinal Effects of Ketamine on Dendritic Architecture In Vivo in the Mouse Medial Frontal Cortex123. *Eneuro* 3: ENEURO.0133-15.2016.
61. Perrin-Terrin A-S, Jeton F, Pichon A, Frugière A, Richalet J-P, Bodineau L, Voituron N (2016): The c-FOS Protein Immunohistological Detection: A Useful Tool As a Marker of Central Pathways Involved in Specific Physiological Responses In Vivo and Ex Vivo. *J Vis Exp*. https://doi.org/10.3791/53613
62. Joo J-Y, Schaukowitch K, Farbiak L, Kilaru G, Kim T-K (2016): Stimulus-specific combinatorial functionality of neuronal c-fos enhancers. *Nat Neurosci* 19: 75–83.
63. Lee J, Urban-Ciecko J, Park E, Zhu M, Myal SE, Margolis DJ, Barth AL (2021): FosGFP expression does not capture a sensory learning-related engram in superficial layers of mouse barrel cortex. *Proc National Acad Sci* 118: e2112212118.
64. Jackson ME, Homayoun H, Moghaddam B (2004): NMDA receptor hypofunction produces concomitant firing rate potentiation and burst activity reduction in the prefrontal cortex. *Proc National Acad Sci* 101: 8467–8472.
65. Ali F, Gerhard DM, Sweasy K, Pothula S, Pittenger C, Duman RS, Kwan AC (2020): Ketamine disinhibits dendrites and enhances calcium signals in prefrontal dendritic spines. *Nat Commun* 11: 72.
66. Nishizawa N, Nakao S, Nagata A, Hirose T, Masuzawa M, Shingu K (2000): The effect of ketamine isomers on both mice behavioral responses and c-Fos expression in the posterior cingulate and retrosplenial cortices. *Brain Res* 857: 188–192.
67. Vesuna S, Kauvar IV, Richman E, Gore F, Oskotsky T, Sava-Segal C, *et al.* (2020): Deep posteromedial cortical rhythm in dissociation. *Nature* 586: 87–94.
68. Aghajanian GK, Hailgler HJ (1975): Hallucinogenic indoleamines: Preferential action upon presynaptic serotonin receptors. *Psychopharmacol Comm* 1: 619–29.
69. Craig AD (Bud) (2009): How do you feel — now? The anterior insula and human awareness. *Nat Rev Neurosci* 10: 59–70.
70. Zheng Z, Guo C, Li M, Yang L, Liu P, Zhang X, *et al.* (2022): Hypothalamus-habenula potentiation encodes chronic stress experience and drives depression onset. *Neuron*. https://doi.org/10.1016/j.neuron.2022.01.011
71. Yang Y, Cui Y, Sang K, Dong Y, Ni Z, Ma S, Hu H (2018): Ketamine blocks bursting in the lateral habenula to rapidly relieve depression. *Nature* 554: 317–322.

72. Proulx CD, Hikosaka O, Malinow R (2014): Reward processing by the lateral habenula in normal and depressive behaviors. *Nat Neurosci* 17: 1146–1152.
73. Gerhard DM, Pothula S, Liu R-J, Wu M, Li X-Y, Girgenti MJ, *et al.* (2019): GABA interneurons are the cellular trigger for ketamine's rapid antidepressant actions. *J Clin Invest* 130: 1336–1349.
74. Tasic B, Yao Z, Graybuck LT, Smith KA, Nguyen TN, Bertagnolli D, *et al.* (2018): Shared and distinct transcriptomic cell types across neocortical areas. *Nature* 563: 72–78.
75. Michaiel AM, Parker PRL, Niell CM (2019): A Hallucinogenic Serotonin-2A Receptor Agonist Reduces Visual Response Gain and Alters Temporal Dynamics in Mouse V1. *Cell Reports* 26: 3475-3483.e4.
76. Bonapersona V, Schuler H, Damsteegt R, Adolfs Y, Pasterkamp RJ, Heuvel MP van den, *et al.* (2022): The mouse brain after foot shock in four dimensions: Temporal dynamics at a single-cell resolution. *Proc National Acad Sci* 119: e2114002119.
77. Roth BL, Lopez E, Patel S, Kroeze WK (2000): The Multiplicity of Serotonin Receptors: Uselessly Diverse Molecules or an Embarrassment of Riches? *Neurosci* 6: 252–262.
78. Meltzer-Brody S, Colquhoun H, Riesenberg R, Epperson CN, Deligiannidis KM, Rubinow DR, *et al.* (2018): Brexanolone injection in post-partum depression: two multicentre, double-blind, randomised, placebo-controlled, phase 3 trials. *Lancet* 392: 1058–1070.
79. Calabrese JR, Durgam S, Satlin A, Vanover KE, Davis RE, Chen R, *et al.* (2021): Efficacy and Safety of Lumateperone for Major Depressive Episodes Associated With Bipolar I or Bipolar II Disorder: A Phase 3 Randomized Placebo-Controlled Trial. *Am J Psychiat* 178: 1098–1106.
80. Davoudian PA, Wilkinson ST (2020): Chapter Four Clinical overview of NMDA-R antagonists and clinical practice. *Adv Pharmacol* 89: 103–129.
81. Hecking J, Davoudian PA, Wilkinson ST (2021): Emerging Therapeutics Based on the Amino Acid Neurotransmitter System: An Update on the Pharmaceutical Pipeline for Mood Disorders. *Chronic Stress* 5: 24705470211020450.
82. Nagele P, Duma A, Kopec M, Gebara MA, Parsoei A, Walker M, *et al.* (2015): Nitrous Oxide for Treatment-Resistant Major Depression: A Proof-of-Concept Trial. *Biol Psychiat* 78: 10–18.